PHYSICAL REVIEW E **91**, 042808 (2015)

Eigenspectrum bounds for semirandom matrices with modular and spatial structure for neural networks

Dylan R. Muir* and Thomas Mrsic-Flogel
Biozentrum, University of Basel, 4056 Basel, Switzerland
(Received 1 September 2014; revised manuscript received 16 January 2015; published 24 April 2015)

The eigenvalue spectrum of the matrix of directed weights defining a neural network model is informative of several stability and dynamical properties of network activity. Existing results for eigenspectra of sparse asymmetric random matrices neglect spatial or other constraints in determining entries in these matrices, and so are of partial applicability to cortical-like architectures. Here we examine a parameterized class of networks that are defined by sparse connectivity, with connection weighting modulated by physical proximity (i.e., asymmetric Euclidean random matrices), modular network partitioning, and functional specificity within the excitatory population. We present a set of analytical constraints that apply to the eigenvalue spectra of associated weight matrices, highlighting the relationship between connectivity rules and classes of network dynamics.

DOI: 10.1103/PhysRevE.91.042808 PACS number(s): 84.35.+i, 87.18.Sn, 02.10.Yn, 87.19.lj

I. INTRODUCTION

The distribution and magnitude of the eigenvalues of random matrices arise in the analysis of many physical systems, and are of particular interest in theoretical neuroscience. The eigenspectrum of the weighted coupling matrix W of a neural network provides valuable information concerning the stability and behavior of a simulated model [1–6]: for example, the magnitude of the eigenvalue with the largest real part places limits on the linear stability of a network or of network partitions [1,3,5,7]; the existence and magnitude of complex eigenvalues determine whether oscillatory network dynamics are expressed [4,8–10]. Numerically computing eigenvalues for small networks is trivial, but analytical eigenvalue solutions for matrices corresponding to even small nonsymmetric networks with relatively simple structure rapidly become intractable [10].

Weight matrices for large networks are often generated randomly, and so theorems concerning the eigenvalue spectra of random nonnegative matrices [11,12] and random matrices with positive-only and negative-only columns apply [2,13,14]. However, connections in physical systems such as the mammalian neocortex are not made randomly [15–22] and include spatial constraints, and so these theorems are insufficient for models with more cortically realistic architecture. Here we propose two alternative rule-based methods for generating matrices corresponding to systems with parameterized nonrandom interactions, and determine bounds on the eigenvalue spectra of these matrices.

We begin by designing a family of sparse asymmetric matrices which include community structure, as well as constraints inherited from Euclidean random matrices. These matrices describe connectivity within directed, weighted networks. We first derive bounds on the maximum real eigenvalues for matrices with stochastic community structure. We follow by deriving bounds on the maximum real eigenvalues for sparse asymmetric Euclidean random matrices, which describe networks with smooth spatial connectivity constraints. Finally we discuss the implications of our results for neocortex.

II. NETWORK ARCHITECTURE

Many networks describing biological phenomena incorporate weighted, signed interactions between nodes, for example, gene regulatory networks [23], activator-inhibitor systems [24], or biological neural networks [25]. Here we model such systems by imposing a blocked sign structure on a matrix defining the strength of pairwise interaction between nodes. A network of N nodes consists of a number $f_I N$ of inhibitory nodes and $(1 - f_I)N$ excitatory nodes, where f_I is the proportion of inhibitory nodes in the network ($0 \leqslant f_I \leqslant 1$). Excitatory nodes form strictly positive connections, and inhibitory nodes form strictly negative connections. The resulting connection weight matrix W is partitioned as

$$W = \begin{bmatrix} B_E & B_I \end{bmatrix} = \begin{bmatrix} W_{EE} & -W_{EI} \\ W_{IE} & -W_{II} \end{bmatrix}, \tag{1}$$

where all entries w_{ij} in W_{EE}, W_{EI}, W_{IE}, and W_{II} are $\geqslant 0$. W_{EE} has $(1 - f_I)N \times (1 - f_I)N$ elements; W_{IE} has $f_I N \times (1 - f_I)N$ elements; W_{EI} has $(1 - f_I)N \times f_I N$ elements; W_{II} has $f_I N \times f_I N$ elements; and B_E and B_I, respectively, denote the excitatory and inhibitory blocks of W.

A. Stochastic community structure

Many man-made and biological networks contain clustering of connections, such that "communities" of nodes which are more tightly coupled emerge [26]. In mammalian neocortex, for example, connections between neurons in the cortex are not made randomly, even ignoring any dependence on physical location. Excitatory neurons in the rodent cortex form subnetworks within which connections are made more densely [20,21,27]. We include this constraint by defining a number of subnetwork blocks, M, that equally partition the excitatory population. Each excitatory node i is assigned to a subnetwork with ID $v_i : (1..M)$, with each subnetwork containing $(1 - f_I)N/M$ excitatory nodes. We define the elements of the subnetwork block membership matrix as

*dylan.muir@unibas.ch; http://dylan-muir.com

$q_{m;ji} \in Q_m$, where

$$q_{m;ji} = \begin{cases} 1 & \text{if } v_i = v_j = m \text{ and } i,\ j \text{ are excitatory} \\ 0 & \text{otherwise} \end{cases}.$$

The matrix Q_m is therefore a $N \times N$ boolean matrix indicating possible excitatory to excitatory connections within a single subnetwork m. We also define the matrix $\mathbf{Q} = (\cup_M Q_m)M/N$, where $\cup_M Q_m$ is the elementwise boolean OR of all matrices Q_m. The submatrix $\mathbf{Q}_{EE}$ then refers to the portion of $\mathbf{Q}$ describing block membership within the population of excitatory nodes.

Connections within and between subnetworks are governed by a global parameter r, which defines the proportion of total connections weight for each excitatory node that is restricted to be made within each subnetwork (with $0 \leqslant r \leqslant 1$).

B. Spatial and functional connectivity constraints

Pairwise interactions in physical networks can depend on distance, such that the strength or probability of interaction is related to physical distance via a function over Euclidean space. Random matrices that incorporate this constraint are known as Euclidean random matrices [28], and have been used to model physical phenomena such as diffusion [29] and wave propagation [30]. Neurons in the neocortex reside in physical space, with connection probabilities modulated smoothly across the cortical surface [31–33]. In addition, connections within the cortex are modulated by functional similarity over one or more physiological metrics. For example, in the primary visual cortex of many mammals the response of a neuron to a set of drifting grating stimuli can be highly tuned to the orientation or direction of grating drift [34]. In many mammalian species, neurons (or small regions of the cortex) that have similar functional metrics are more likely to be connected (mouse, [21]; cat, [15,22]; tree shrew, [19]; monkey, [17,18,22]; human, [16]). For simplicity, we consider that these functional dimensions are treated similarly to spatial dimensions, so that a node is assigned a "location" in a high-dimensional space that defines its spatial and functional properties. As an alternative form of nonrandom connectivity in addition to the stochastic community structure described above, we consider systems where connectivity is smoothly modulated according to spatial and functional constraints.

Each node i is randomly assigned a location vector $\mathbf{x}_i$ sampled uniformly from the unit hypercube with dimensionality D, such that $\mathbf{x}_i = \{x_{i,1}, x_{i,2}, \ldots, x_{i,D}\}$ and $x_{i,k} \sim \text{Uniform}(0,1)$. The matrix $s_{ji} \in S$, which contains connection weights defined by spatial and functional relationships, is a Euclidean random matrix with $s_{ji} = \mathscr{F}(\mathbf{x}_i, \mathbf{x}_j)$, where $\mathscr{F}(\cdot)$ is a function defining the connection weight according to a similarity metric relating the location of nodes i and j [28].

In this work we consider a smooth connectivity relationship in a multidimensional space, under the assumption that the space in which the network resides is a hypertorus, such that the opposite planes along each axis are contingent. As a connectivity relationship we adopt a D-dimensional Gaussian, such that

$$\mathscr{F}(\mathbf{x}_i, \mathbf{x}_j) = \mathscr{G}(\|\mathbf{x}_i - \mathbf{x}_j\|^\circ) = \exp\left(-\frac{\|\mathbf{x}_i - \mathbf{x}_j\|^{\circ 2}}{D^2\kappa^2}\right), \quad (2)$$

where $\|\mathbf{x}_i - \mathbf{x}_j\|^{\circ 2}$ is the squared two-norm distance over a unit hypertorus, given by

$$\|\mathbf{x}_i - \mathbf{x}_j\|^{\circ 2} = \sum_{d=1..D} (\arccos\{\cos[2\pi(x_{i,d} - x_{j,d})]\}/2\pi)^2. \quad (3)$$

The connectivity function in Eq. (2) is under the control of a parameter κ, which determines the range of connectivity within the network ($\kappa > 0$). As κ increases, so does the spatial and functional range over which connections are distributed. The matrix S is normalized such that it approximates a discrete probability density function (PDF) of the connections to each node, i.e., $\mathrm{E}[\Sigma\Sigma S] = N$.

C. Sparse connectivity

Connectivity in many networks is extremely sparse, whereby a node is connected to only a few of its potential partners. We include this constraint by defining fill factors h_E and h_I, which determine the proportion of nonzero connections in B_E and B_I, respectively ($0 < h_E \leqslant 1; 0 < h_I \leqslant 1$) [2]. For a given network, a sparse boolean matrix C defines which connections are randomly selected to exist, where $c_{ji} \in C$ defines the presence or absence of a connection from node i to node j. In practice, we define the matrix C by randomly distributing the appropriate number of zero values in each column of the submatrices C_{EE}, C_{EI}, C_{IE}, and C_{II}. For small κ and small N, self-connections have a large impact on the eigenvalues and network stability. The influence of diagonal elements of W decreases as $\kappa \to \infty$ and as $N \to \infty$. In the limit as $N \to \infty$, elements of C can be assumed to be independent, and therefore approximated by a Bernoulli distribution.

D. Composed network connection matrix

We define the family of random matrices examined in this work as

$$W = C \otimes \begin{bmatrix} W_{EE} = w_E(r \cdot \mathbf{Q}_{EE} + (1-r)S_{EE})h_E^{-1} & -W_{EI} = -w_I \cdot S_{EI} \cdot h_I^{-1} \\ W_{IE} = w_E \cdot S_{IE} \cdot h_E^{-1} & -W_{II} = -w_I \cdot S_{II} \cdot h_I^{-1} \end{bmatrix}, \quad (4)$$

where $A \otimes B$ denotes elementwise multiplication between matrices. The expected sum of each column of B_E is equal to w_E (and each column of B_I is equal to $-w_I$).

III. EIGENVALUE SPECTRA OF SPARSE MATRICES WITH STOCHASTIC COMMUNITY STRUCTURE

We first examine the distribution of eigenvalues under the simple stochastic partitioning of networks given by $r > 0$, and ignoring spatial constraints (i.e., $\kappa \to \infty$ and $\forall i, j : [s_{ji} \in S, s_{ji} = \frac{1}{N}]$).

The weight matrix W has a trivial eigenvalue $\lambda_b = w_E(1 - f_I) - w_I f_I$, determined by the global balance between excitation and inhibition in the network [2,10] and which corresponds to the growth rate of a uniform perturbation of network activity [6] [Fig. 1(a)]. This eigenvalue is robust to changes in network size, subnetwork structure, and sparsity. For a full matrix without subnetwork structure (i.e., $h_E = h_I = 1, r = 0$), all other eigenvalues are zero.

Including modular structure of the kind described above introduces a number of nonzero, positive eigenvalues related to the number of subnetworks M and the strength r of within-subnetwork connectivity. W_{EE} can be transformed to a block matrix by grouping excitatory neurons within the same subnetwork, so that

$$W_{EE} = \begin{bmatrix} W_{SSN} & W_{NS} & \cdots & W_{NS} \\ W_{NS} & W_{SSN} & & W_{NS} \\ \vdots & & \ddots & \vdots \\ W_{NS} & W_{NS} & \cdots & W_{SSN} \end{bmatrix},$$

with columns of W_{SSN} summing to $\Sigma W_{SSN} = w_E(1 - f_I)r + w_E(1 - f_I)(1 - r)M^{-1}$ and columns of off-diagonal blocks W_{NS} summing to $\Sigma W_{NS} = w_E(1 - f_I)(1 - r)M^{-1}$. For a nonsparse network, the block structure of W_{EE} therefore introduces $M - 1$ eigenvalues located at $\lambda_Q = \Sigma W_{SSN} - \Sigma W_{NS} = w_E(1 - f_I)r$ that persist as eigenvalues of W [Fig. 1(b)] [35].

As connectivity in the network becomes more sparse (i.e., $h_E, h_I < 1$) and as $N \to \infty$ then the nontrivial and nonsubnetwork eigenvalues become densely clustered within a circle centered at the origin, bounded in expectation by an outer radius related to the variances of the elements of B_E and B_I and given by $\{N[(1 - f_I)\sigma_E^2 + f_I\sigma_I^2]\}^{\frac{1}{2}}$ [Fig. 1(c)] [2]. The subnetwork-related eigenvalues $\lambda_{Q,k}$ become distributed within a circle of radius $\sigma_{\mathbf{Q}}$ centered at λ_Q, where $\sigma_{\mathbf{Q}}$ is the standard deviation of the subnetwork-only connections within W_{EE}, i.e., for which $v_i = v_j$ [Fig. 1(c)].

The elements of B_E have a known discrete distribution, determined by w_E, r, h_E, f_I, and M. Elements of B_E can adopt only three values: zero with probability $(1 - h_E)$; within-subnetwork weights $w_{v_i=v_j} = w_E r M/h_E N + (1 - r)w_E/h_E N$ with probability $p_{v_i=v_j} = h_E(1 - f_I)/M$; excitatory weights with nonsubnetwork partners $w_{v_i\neq v_j} = (1 - r)w_E/h_E N$ with probability $p_{v_i\neq v_j} = h_E(1 - f_I)(1 - 1/M)$; and excitatory to inhibitory weights $w_{EI} = w_E/h_E N$ with probability $p_{EI} = f_I h_E$.

We therefore derive the following analytical expressions for the variance measures of the matrix W. The mean of B_E is given by $\mu_{W_E} = w_E/N$; the mean of within-subnetwork weights (elements of W_{EE} for which $v_i = v_j$) is given by $\mu_{v_i=v_j} = w_E r M/N + (1 - r)w_E/N$. The variance $\sigma_{\mathbf{Q}}^2$ of within-subnetwork connections is therefore given by

$$\sigma_{\mathbf{Q}}^2 = h_E\left(w_{v_i=v_j} - \mu_{v_i=v_j}\right)^2 + (1 - h_E)\mu_{v_i=v_j}^2. \quad (5)$$

Similarly, the variance σ_E^2 of B_E is given by

$$\sigma_E^2 = (1 - h_E)\mu_{W_E}^2 + p_{v_i=v_j}\left(w_{v_i=v_j} - \mu_{W_E}\right)^2 + p_{v_i\neq v_j}\left(w_{v_i\neq v_j} - \mu_{W_E}\right)^2 + p_{EI}(w_{EI} - \mu_{W_E})^2 \quad (6)$$

and the variance σ_I^2 of B_I is given by

$$\sigma_I^2 = (1 - h_I)(w_I/N)^2 + h_I(w_I/h_I N - w_I/N)^2. \quad (7)$$

We therefore obtain closed-form bounds on the eigenvalue spectra for matrices describing sparse networks with stochastic community structure, as $N \to \infty$. The maximum eigenvalue [see Fig. 1(d)] is expected to be smaller than

$$\max\left(\lambda_b, \lambda_Q + \sigma_{\mathbf{Q}}, \left\{N\left[(1 - f_I)\sigma_E^2 + f_I\sigma_I^2\right]\right\}^{\frac{1}{2}}\right). \quad (8)$$

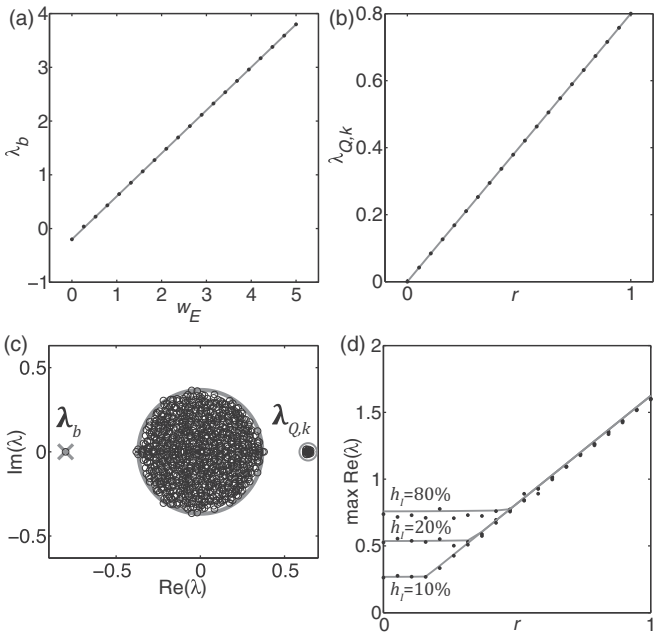

FIG. 1. Empirical and analytical eigenvalue distributions are closely matched. (a) Analytical predictions of λ_b (curve) match empirical observations (dots) in a sparse network without community structure with $N = 500$, $h_E = 10\%$, $h_I = 50\%$, $w_I = -1$, and $f_I = 20\%$. (b) Analytical predictions of λ_Q (curve) match empirical observations (dots) in a full network (i.e., h_E,$h_I = 100\%$) with $N = 500$, $w_E = 1$, $w_I = -10$, $f_I = 20\%$, and with two subnetwork partitions ($M = 2$). (c) The distribution of empirical eigenvalues (black circles) matches the analytical bounds (gray circles and markers) in a sparse network ($N = 1000$, $h_E = 10\%$, and $h_I = 50\%$) with many subnetwork partitions ($M = 20$) and with $w_E = 2$, $w_I = -12$, $f_I = 20\%$. (d) Analytical predictions of the maximum real eigenvalue max Re(λ) (curves) correspond well to the empirical maximum real eigenvalue, in a sparse network ($N = 5000$, $h_E = 10\%$, $h_I = \{10\%, 20\%, 80\%\}$) containing two subnetwork partitions ($M = 2$) and with $w_E = 2$, $w_I = -12$, $f_I = 20\%$, and $h_E = 10\%$.

IV. EIGENVALUES OF MATRICES DESCRIBING NETWORKS WITH SPATIAL CONNECTIVITY CONSTRAINTS

We now examine the eigenvalues of matrices describing networks that include a connection constraint over spatial proximity or functional similarity, with $r = 0$.

In the degenerate limit where $\kappa \to 0$ (and assuming $h = 1$), each node in the network connects only to itself. This results in a diagonal matrix W with all-zero off-diagonal entries, $(1 - f_I)N$ diagonal entries equal to w_E and $f_I N$ diagonal entries equal to w_I. As a consequence all eigenvalues of W are real, with $(1 - f_I)N$ eigenvalues at w_E and $f_I N$ eigenvalues at $-w_I$. In the other limit, as $\kappa \to \infty$, connection weighting according to spatial and functional similarity becomes uniform and the solutions derived for nonspatial networks in the previous section apply.

For finite N and $0 < \kappa < \infty$, the connection profile imposed by Eq. (2) serves to strongly couple each node to a group of nearby nodes, with the size of the group decreasing as $\kappa \to 0$. We estimate the eigenvalue distribution produced by the influence of this spatial restriction by approximating a portion of W for a small strongly coupled partition by a pair of excitatory and inhibitory neurons [4], with

$$W|^P = \begin{bmatrix} W_{EE}|^P & -W_{EI}|^P \\ W_{IE}|^P & -W_{II}|^P \end{bmatrix} \approx \begin{bmatrix} \hat{w}_{ee} & -\hat{w}_{ei} \\ \hat{w}_{ie} & -\hat{w}_{ii} \end{bmatrix}, \quad (9)$$

where $\hat{w}_*$ denotes estimates for the means of the corresponding submatrices in $W|^P$. The eigenvalues of $W|^P$ have the form $2\lambda_\pm = \hat{w}_{ee} - \hat{w}_{ii} \pm [(\hat{w}_{ee} + \hat{w}_{ii})^2 - 4\hat{w}_{ei}\hat{w}_{ie}]^{\frac{1}{2}}$.

We obtain closed-form estimates for the distribution of $\{\lambda_+, \lambda_-\}$ over instances of W by examining the most extreme values of $\hat{w}_*$. We denote the maximum estimate of a parameter by $\lceil\cdot\rceil$, and the minimum estimate as $\lfloor\cdot\rfloor$. We estimate the eigenspectrum bounds as

$$\begin{aligned} 2\lceil\lambda_+\rceil &= \lceil\hat{w}_{ee}\rceil - \lfloor\hat{w}_{ii}\rfloor + [(\lceil\hat{w}_{ee}\rceil + \lfloor\hat{w}_{ii}\rfloor)^2 - 4\lceil\hat{w}_{ie}\rceil\lfloor\hat{w}_{ei}\rfloor]^{\frac{1}{2}}, \\ 2\lfloor\lambda_-\rfloor &= \lfloor\hat{w}_{ee}\rfloor - \lceil\hat{w}_{ii}\rceil - [(\lfloor\hat{w}_{ee}\rfloor + \lceil\hat{w}_{ii}\rceil)^2 - 4\lfloor\hat{w}_{ie}\rfloor\lceil\hat{w}_{ei}\rceil]^{\frac{1}{2}}. \end{aligned} \quad (10)$$

To obtain estimates for $\hat{w}_*$, we derive the distribution of sums of elements of S. The mean and variance of elements $s \in S$ are given by

$$\begin{aligned} \mathrm{E}[s] &= \iint_D \mathscr{G}(\|\mathbf{x} - \mathbf{0}\|^\circ) d\mathbf{x} \\ &= D^D \pi^{D/2} \kappa^D \mathrm{erf}(1/2D\kappa)^D, \end{aligned} \quad (11)$$

$$\begin{aligned} \sigma_s^2 &= \iint_D \mathscr{G}^2(\|\mathbf{x} - \mathbf{0}\|^\circ) d\mathbf{x} - \mathrm{E}^2[s] \\ &= D^D (\pi/2)^{D/2} \kappa^D \mathrm{erf}(1/\sqrt{2}D\kappa)^D - \mathrm{E}^2[s], \end{aligned} \quad (12)$$

where $\mathrm{E}[\cdot]$ is the expectation operator. By transforming the distributions of variates used to compose S, we observe that the sum of L elements in S (defined as $\Sigma_L S$) is distributed as $\Sigma_L S \sim \mathrm{Gamma}(\alpha_D, \theta_D)$, with $\alpha_D = L\,\mathrm{E}^2[s]/\sigma_s^2$ and $\theta_D = \sigma_s^2/\{\mathrm{E}^2[s](N-1) + \mathrm{E}[s]\}$ (see Appendix A). The extremal values of sums $\Sigma_L S$ for $i \neq j$ [see Fig. 2(a)] are then distributed according to

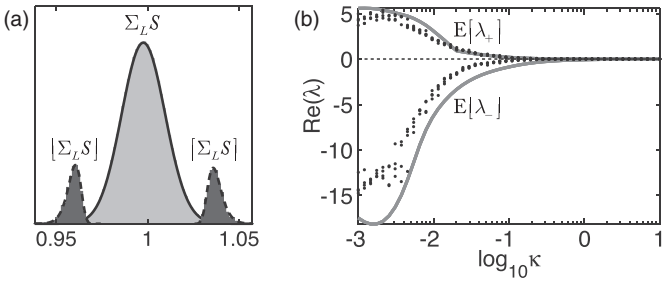

FIG. 2. (a) Analytical distributions of $\Sigma_L S_{i\neq j}$, $\lceil\Sigma_L S_{i\neq j}\rceil$, and $\lfloor\Sigma_L S_{i\neq j}\rfloor$ (curves) closely match empirical measurements over 2000 network instances (shaded histograms). Network parameters: $N = 1200$, $L = 1199$, $\kappa_s = \frac{1}{8}$, $D = 5$. (b) Analytical predictions of eigenspectra bounds $\mathrm{E}\lceil\lambda_+\rceil$ and $\mathrm{E}\lfloor\lambda_-\rfloor$ (curves) and empirical maximum and minimum eigenvalues (dots) for networks with $r = 0$, $h_I, h_E = 1$, $f_I = 20\%$, $N = 6000$, $D = 2$, $w_E = 2$, and $w_I = 8$.

$$\begin{aligned} \lceil\Sigma_L S_{i\neq j}\rceil &\sim \frac{\Gamma_G\left(\alpha_D, 0, \frac{x}{\theta_D}\right)^{L-1}}{\Gamma(\alpha_D)} \exp\left(\frac{-x}{\theta_D}\right) L x^{-1+\alpha_D} \theta_D^{-\alpha_D}, \\ \lfloor\Sigma_L S_{i\neq j}\rfloor &\sim \frac{\Gamma_R\left(\alpha_D, \frac{x}{\theta_D}\right)^{L-1}}{\Gamma(\alpha_D)} \exp\left(\frac{-x}{\theta_D}\right) L x^{-1+\alpha_D} \theta_D^{-\alpha_D}, \end{aligned} \quad (13)$$

where the notation $\vartheta \sim P(x)$ indicates that ϑ is distributed proportional to function $P(x)$, with a suitable normalization factor such that $P(x)$ forms a valid probability density function. In Eq. (13), $\Gamma(z)$ is the Euler gamma function, $\Gamma_G(a, z_0, z_1) = \Gamma_R(a, z_0) - \Gamma_R(a, z_1)$ is the generalized regularized incomplete gamma function, $\Gamma_R(a, z) = \Gamma(a)^{-1} \int_z^\infty t^{a-1} \exp(-t) dt$ is the regularized upper incomplete gamma function, and α_D and θ_D are the shape and scale parameters of the gamma distribution, given above.

The partition estimates for the case when $r = 0$ (i.e., only spatial constraints are considered) are described by $\hat{w}_{ee} \sim w_E(s_{ii} + \Sigma_{(1-f_I)N-1} S)$, $\hat{w}_{ii} \sim w_I(s_{ii} + \Sigma_{f_I N - 1} S)$, $\hat{w}_{iw} \sim w_E(\Sigma_{f_I N} S)$, and $\hat{w}_{ei} \sim w_I(\Sigma_{(1-f_I)N} S)$, where $\Sigma_L S$ is the sum of L elements $s_{ji} \in S$ for $i \neq j$, and $s_{ii} \equiv S_{i=j} = \{\mathrm{E}[s](N-1) + 1\}^{-1}$. The extremal value expectations $\mathrm{E}\lceil\hat{w}_*\rceil$ and $\mathrm{E}\lfloor\hat{w}_*\rfloor$ are used to estimate the bounds in Eq. (10) [an example is shown in Fig. 2(b)].

When sparse connections are included (i.e., $h_E, h_I < 1$), the maximum eigenvalue of W for large N is estimated by

$$\max\left(\lambda_b, \left\{N\left[(1 - f_I)\sigma_E^2 + f_I \sigma_I^2\right]\right\}^{\frac{1}{2}}, \lceil\lambda_+\rceil\right). \quad (14)$$

V. DISCUSSION

The eigenvalue spectrum bounds we derived for asymmetric matrices apply equally to symmetric Euclidean random matrices defined by a Gaussian function on a torus, as can be obtained by letting $f_I = 0$. In this case, the maximum real eigenvalue is estimated by $\lceil\lambda_+\rceil = \mathrm{E}\lceil\hat{w}_{ee}\rceil$, and an analytical probability distribution for λ_+ is given in Eq. (13). Closed bounds can be obtained for these eigenvalues, as opposed to the bounds in expectation derived here, if connection

functions with bounded domains are used for $\mathscr{F}(\cdot)$ in Eq. (2).

Results describing eigenvalue distributions for unweighted, unsigned, and undirected random graphs with hierarchical community structure will apply to the portion of **Q** that corresponds to the excitatory portion of W [35–38]. These results suggest that methods for spectral identification of modular structure might be applicable to biological networks, if dense and relatively complete connectivity matrices can be obtained experimentally [35,39–41]. Although our results apply instead to the signed and weighted connectivity matrix W, we found that the blocking structure is nevertheless reflected in the closed-form expression for the bounds on eigenvalues λ_Q.

We examined a partitioning of W where subnetworks were of equal size, a reasonable assumption for cortical networks with large N. If the size of each subnetwork is allowed to vary, then the magnitude of the associated eigenvalues will change with group size [35]. However, the precise value of each eigenvalue will then depend crucially on how the total weight within each subnetwork is normalized.

Implications for dynamics and computation in neural networks and in the cortex

Here we briefly discuss the implications of our eigenspectra results for the behavior of neural networks, where the matrix W defines the connection weights within a sparsely connected network, and where the transfer function of each node is approximated by a linear or threshold-linear function. Our results are suggestive of stability and operating regimes also for networks with nonlinear transfer functions, but the shape of the neuron gain function can introduce further complexity into the operating modes of a network [42,43].

For all networks regardless of nonrandom structure, the eigenvalue λ_b determined by the global balance between excitation and inhibition limits the global stability of a neural network under the constraint $\lambda_b \leqslant 1$ [2,6,10].

In networks with modular (or "community" or "planted partition") structure, the subnetwork eigenvalues $\lambda_{Q,k}$ (for $k = 1..M-1$) correspond to eigenvectors that express competition between subnetwork partitions of the excitatory network. The presence of these eigenvectors implies that if a subnetwork partition is active it will tend to decrease the activity of the other excitatory subnetworks. If these eigenvalues correspond to unstable modes (i.e., $\lambda_Q > 1$) then the competition eigenvectors are unstable and the corresponding nonlinear network will be characterized by hard competitive interactions between subnetworks [10,44]. However, this need not lead to overall network instability. Due to the threshold nonlinearity present in most neural simulations, the unstable competitive modes of the network will silence one or more of the "losing" subnetwork partitions, modifying the stability structure of the network [1]. Under the symmetric and balanced modular architecture discussed here, eventually only a single excitatory subnetwork partition will remain active. The matrix W can then be reduced to a two-element equivalent to a single partition, similar to the treatment used in Eq. (9), with $W|^P = \left[\begin{smallmatrix} w_{SSN} & -w_I f_I \\ w_E f_I & -w_I f_I \end{smallmatrix}\right]$, where $w_{SSN} = w_E(1-f_I)(r+[1-r]M^{-1})$. This network partition is stable under the conditions $w_{SSN} < 2 + w_I f_I$ and $w_E f_I \leqslant (w_{SSN} + w_I f_I)^2 (4 w_I f_I)^{-1}$. Competition will therefore silence all but one subnetwork through the action of disynaptic inhibition; this form of network dynamics is probably undesirable in the cortex. Our results indicate that in the absence of an inhibitory contribution to subnetwork membership the subnetwork eigenvalues λ_Q are not dependent on global inhibitory feedback. Due to the structure of λ_Q, increasing the strength of inhibition cannot therefore balance the effect of introducing modular connectivity to a network. This surprising result suggests that hard limits exist on the degree of subnetwork specificity allowable for synaptic connections in the cortex.

Previous results have derived Eigenvalue spectra for Hermitian and non-Hermitian Euclidean random matrices by forming analytical decompositions of the spatial operator resolvent [30,45], but have not analyzed matrices with block-signed structure similar to those we discuss here. Our results for networks with smooth spatial and functional connectivity indicate that in Euclidean random matrices including a signed bipartition of positive and negative elements the bound of the eigenspectrum becomes increasingly sensitive to the local balance between positive and negative interactions as the spatial range of interactions decreases. Interpreted for cortical architecture, our result implies that as connections become more functionally and spatially constrained networks become increasingly sensitive to the local balance between excitation and inhibition, in the form of excitatory recurrence ($\hat{w}_{ee}$) and excitatory or inhibitory recurrent connections $\hat{w}_{ie}$ and $\hat{w}_{ei}$. This is because feedback within the network is restricted to ever-smaller subpopulations, and random deviations away from expected values of connectivity cannot be effectively averaged away. These issues decrease in severity for large N, but are exacerbated in extremely sparse networks such as the mammalian neocortex (i.e., $h_E, h_I \to 0$). Our results highlight the importance of excitatory and inhibitory balance, not only globally but also at the mesoscale of local network statistics. Since our connectivity constraints can be treated as functional similarity constraints over some physiological measure, we expect that homeostatic plasticity mechanisms in the cortex must be sensitive to balance within functional cohorts.

ACKNOWLEDGMENTS

We thank L. Cossell, A. Landsman, M. Pfeiffer, M. Penny, M. Okun, and P. Latham for helpful discussions. This work was supported by the University of Basel Young Researchers fund.

APPENDIX A: ANALYTICAL PROBABILITY DISTRIBUTIONS FOR UNIFORM RANDOM LOCATIONS AND GAUSSIAN FUNCTIONS OF DISTANCE ON A D-DIMENSIONAL TORUS

1. Distribution of squared distances between uniform random variates

The Euclidean distance measures on a torus used to generate the weight distributions in the body of the paper are examined

TABLE I. Parameter estimates for truncated Rice distribution Rice(σ_D, ν_D) approximations to Δ_D^2. The support of Δ_D^2 is $0 < x < \frac{D}{4}$.

D	σ_D	ν_D
4	0.171369	0.273127
5	0.181867	0.367747
6	0.194213	0.455956
7	0.206722	0.541939
8	0.218954	0.626903
9	0.230778	0.711325
10	0.242168	0.795430

to determine their analytical distributions. These distributions have a complex form depending on the dimensionality of the space, and there is no general solution. Here we include analytical forms for $D = 1..4$ and analytical approximations for $D > 4$.

We begin by examining the distribution of city-block distances along single dimensions, given by $\delta = \text{acos}\{\cos[2\pi(n_1 - n_2)]\}/2\pi$, where the variates n_1 and n_2 are the uniformly distributed locations of two points along a single dimension—i.e., $n_1, n_2 \sim \text{Uniform}(0,1)$—and acos$(\cdot)$ is the arc cosine function. We note that, due to the torus relationship, distances along single dimensions maintain a uniform distribution, with $\delta \sim \text{Uniform}(0, \frac{1}{2})$.

In a D-dimensional space, the distribution of the sum of D squared variates $\Delta_D^2 = \sum_{i=1}^{D} \delta_i^2$ is important for examining the Gaussian function over a torus [Eq. (2)]. Each variate δ_i describes the city-block distance along a single dimension, and is uniformly distributed as described above. For $D = 1$, $\Delta_1^2 \tilde{\propto} x^{\frac{-1}{2}}$, with support $0 < x < \frac{1}{4}$, mean $\frac{1}{12}$, and variance $\frac{1}{180}$. The notation $x \tilde{\propto} P$ indicates that x is distributed proportional to PDF P, with a suitable normalization factor.

For $D = 2$ we obtain the exact distribution for Δ_2^2, given by

$$\Delta_2^2 \tilde{\propto} \begin{cases} \pi & 0 < x \leqslant \frac{1}{4} \\ 2\,\text{acsc}[2\sqrt{x}] - 2\,\text{acsc}\left[2\left(4 - \frac{1}{x}\right)^{-\frac{1}{2}}\right] & \frac{1}{4} < x < \frac{1}{2} \end{cases} \tag{A1}$$

with support $0 < x < \frac{1}{2}$, mean $\frac{1}{6}$, and variance $\frac{1}{90}$, where acsc(z) is the arc cosecant function of the complex variable z.

For $D = 3$ we obtain the exact distribution for Δ_3^2, given by

$$\Delta_3^2 \tilde{\propto} \begin{cases} 2\pi\sqrt{x} & 0 < x \leqslant \frac{1}{4} \\ \pi(3 - 4\sqrt{x}) & \frac{1}{4} < x \leqslant \frac{1}{2} \\ \pi + 8\sqrt{x}[-\text{acot}(2\sqrt{2}\sqrt{x(2x-1)}) & \\ \quad +\text{acot}\sqrt{1 + 1/(2x-1)}] & \frac{1}{2} < x < \frac{3}{4} \\ \quad +4\,\text{acsc}\sqrt{4x-1} - 8\,\text{atan}\sqrt{4x-2} & \end{cases} \tag{A2}$$

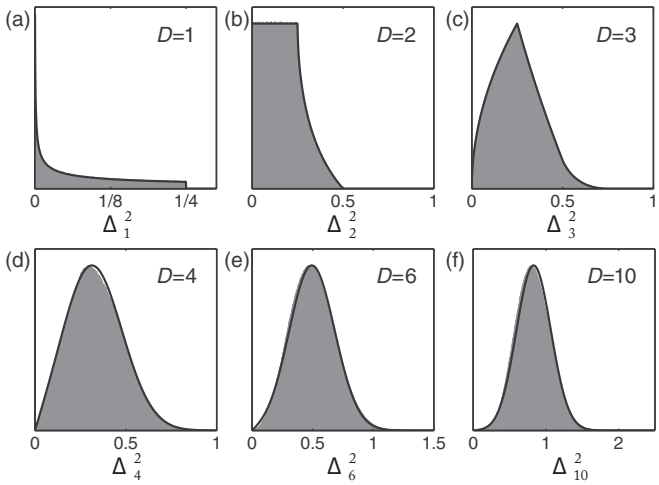

FIG. 3. Analytical and approximate distributions of Δ_D^2. (a–c) Analytical distributions (black) compared against empirical distributions for 5000 variates (shaded histograms). These distributions are exact; note the perfect overlap between empirical and analytical distributions. (d–f) A Rice distribution (black) gives a close approximation to the empirical distribution of Δ_D^2 (shaded histograms) for $D = 4$–10. Values of D are as indicated on the figure.

with support $0 < x < \frac{3}{4}$, mean $\frac{1}{4}$, and variance $\frac{1}{60}$, where atan(x) is the arc tangent function and acot(z) is the arc cotangent function of the complex variable z.

For $D > 3$, Δ_D^2 can be closely approximated by a Rice distribution [46]. An analytical solution for the parameters σ and ν of a Rice distribution for a given mean and variance is not available, but iterative estimation of these parameters is possible [47]. In Table I we provide numerically derived parameter estimates for Rice distribution approximations for $D = 4$–10. Figure 3 shows a comparison between empirical distributions of Δ_D^2 and the analytical approximations described here.

In the general case the support of Δ_D^2 is given by $0 < x < \frac{D}{4}$, the mean is given by $\text{E}[\Delta_D^2] = \frac{D}{12}$, and the variance is given by $\sigma^2_{\Delta_D^2} = \frac{D}{180}$. For $D > 10$, Δ_D^2 can be closely approximated by a normal distribution with $\Delta_D^2 \sim \text{Normal}(\frac{D}{12}, \sqrt{\frac{D}{180}})$.

2. Gaussian function over uniformly distributed locations on a torus

We now examine the distribution of the Gaussian function used in the body of the paper [Eq. (2)] such that $g_D = \mathcal{G}(\Delta_D^2) = \exp(-\Delta_D^2/\kappa^2)$. We obtain closed-form solutions by transforming the probability distributions for Δ_D^2 given above. Generally, $g_D \sim P(a \leqslant y \leqslant b) = \mathcal{G}^{-1}(y) \int_{\mathcal{G}(a)}^{\mathcal{G}(b)} \text{PDF}_{\Delta_D^2}[\mathcal{G}^{-1}(y)] \frac{d}{dy}$, where $\text{PDF}_{\Delta_D^2}[x]$ is the probability density function for Δ_D^2 and $\mathcal{G}^{-1}(y)$ is the inverse of $\mathcal{G}(x)$, given by $\mathcal{G}^{-1}(y) = -\kappa^2 D^2 \sqrt{-\ln y}$.

For $D = 1$ we obtain the simple form $g_1 \tilde{\propto} (x\sqrt{-\ln x})^{-1}$ with support $s_{\kappa,1,1} < x < 1$, where $s_{\kappa,D,l} = \exp[-l/(4D^2\kappa^2)]$. The distribution for g_1 can be closely approximated by a Beta distribution with $g_1 \sim \text{Beta}(1/5, 1/2)$ with the same support as given above.

For $D = 2$ we obtain the exact distribution for g_2, given by

$$g_2 \approx \begin{cases} 8\kappa^2 x^{-1}[\operatorname{acot} c_\kappa(x) - \operatorname{atan} c_\kappa(x)] & s_{\kappa,2,2} < x < s_{\kappa,2,1} \\ 4\pi\kappa^2 x^{-1} & s_{\kappa,2,1} \leqslant x < 1 \end{cases} \tag{A3}$$

with support $s_{\kappa,2,2} < x < 1$ and where $c_\kappa(x) = \kappa\sqrt{-\kappa^{-2} - 16\ln x}$.

For $D = 3$ we obtain the exact distribution for g_3, given by

$$g_3 \approx \begin{cases} 9\kappa^2 x^{-1}(\pi + 4\operatorname{acsc}\sqrt{-1 - 36\kappa^2 \ln x} \\ \quad -8\operatorname{atan}\sqrt{-2 - 36\kappa^2 \ln x} + (24\kappa\sqrt{-\ln x}) \\ \quad \times\{\operatorname{acot}\sqrt{1 + 1/(-1 - 18\kappa^2 \ln x)} \\ \quad -\operatorname{acot}[6\sqrt{2}\kappa\sqrt{\ln x(1 + 18\kappa^2 \ln x)}]\}) & s_{\kappa,2,3} < x < s_{\kappa,2,2} \\ 27\pi\kappa^2 x^{-1}(1 - 4\kappa\sqrt{-\ln x}) & s_{\kappa,2,2} \leqslant x < s_{\kappa,2,1} \\ 54\pi\kappa^3 x^{-1}\sqrt{-\ln x} & s_{\kappa,2,1} \leqslant x < 1 \end{cases} \tag{A4}$$

By using the Rice distribution approximation to Δ_D^2, an approximation to g_D for $D = 4$–10 is given by

$$g_D \approx \frac{D^4\kappa^4 \ln x}{x\nu_D^2} \exp\left(-\frac{\sigma_D^2 + D^4\kappa^4 \ln^2 x}{2\nu_D^2}\right) \times \mathrm{I}_0\left(\frac{D^2\kappa^2\sigma_D \ln x}{\nu_D^2}\right), \tag{A5}$$

where σ_D and ν_D are the approximation parameters from Table I above and $\mathrm{I}_0(\cdot)$ is the zeroth-order modified Bessel function.

Taking the normal distribution approximation to Δ_D^2 for $D > 10$, g_D becomes log-normally distributed with

$$g_D \sim \text{Log normal}[-(12\,D\kappa^2)^{-1}, (6\sqrt{5}D^{\frac{3}{2}}\kappa^2)^{-1}]. \tag{A6}$$

In the general case, the support of the distribution of g_D is given by $s_{\kappa,D,D} < x < 1$. For arbitrary D, the mean and variance of g_D can be obtained by integrating $\mathscr{G}(\cdot)$ [Eq. (2)] and are given by

$$\begin{aligned} \mathrm{E}[g_D] &= \iint_D \mathscr{G}(\|\mathbf{x} - \mathbf{0}\|^\circ)d\mathbf{x} = D^D\pi^{\frac{D}{2}}\kappa^D \mathrm{erf}(1/2D\kappa)^D, \\ \sigma_{g_D}^2 &= \iint_D \mathscr{G}^2(\|\mathbf{x} - \mathbf{0}\|^\circ)d\mathbf{x} - \mathrm{E}^2[g_D] \\ &= D^D(\pi/2)^{D/2}\kappa^D \mathrm{erf}(1/\sqrt{2}D\kappa)^D - \mathrm{E}^2[g_D]. \end{aligned} \tag{A7}$$

3. Extreme value distributions for column sums of B_E and B_I

To obtain limits on the eigenspectra of spatial networks, we require the expected extreme values $\lceil\hat{w}_*\rceil$ and $\lfloor\hat{w}_*\rfloor$ of summed excitation and inhibition within the partition estimates, as discussed in Eqs. (9) and (10) in the body of the paper. Since the elements in B_E and B_I are highly correlated, the central limit theorem does not apply and sums of columns of W are not normally distributed. This caveat applies particularly badly for small D and $\kappa \ll 1$. However, by framing our analysis to apply across many instances of networks we can neglect these correlations and assume that elements of W are independent.

Under the assumption of independence and since the matrix S is appropriately normalized (i.e., $\mathrm{E}[\Sigma S] = N$), sums of L elements of S for $i \neq j$ are distributed according to a gamma distribution $\Sigma_L S_{i\neq j} \sim \text{Gamma}(\alpha_D, \theta_D)$ where $\alpha_D = L\,\mathrm{E}^2[g_D]/\sigma_{g_D}^2$ and $\theta_D = \sigma_{g_D}^2/(\mathrm{E}^2[g_D](N-1) + \mathrm{E}[g_D])$.

The extremal values of sums $\Sigma_L S$ for $i \neq j$ are distributed according to

$$\begin{aligned} \lceil\Sigma_L S_{i\neq j}\rceil &\approx \frac{\Gamma_G(\alpha_D, 0, \frac{x}{\theta_D})^{L-1}}{\Gamma(\alpha_D)} \exp\left(\frac{-x}{\theta_D}\right) L x^{-1+\alpha_D}\theta_D^{-\alpha_D}, \\ \lfloor\Sigma_L S_{i\neq j}\rfloor &\approx \frac{\Gamma_R(\alpha_D, \frac{x}{\theta_D})^{L-1}}{\Gamma(\alpha_D)} \exp\left(\frac{-x}{\theta_D}\right) L x^{-1+\alpha_D}\theta_D^{-\alpha_D}, \end{aligned} \tag{A8}$$

where the estimate of a maximum is denoted by $\lceil\cdot\rceil$ and an estimate of a minimum is denoted by $\lfloor\cdot\rfloor$, $\Gamma(z)$ is the Euler gamma function, $\Gamma_G(a, z_0, z_1) = \Gamma_R(a, z_0) - \Gamma_R(a, z_1)$ is the generalized regularized incomplete gamma function, $\Gamma_R(a, z) = \Gamma(a)^{-1}\int_z^\infty t^{a-1}\exp(-t)dt$ is the regularized upper incomplete gamma function, and α_D and θ_D are the shape and scale parameters of the gamma distribution. Because each neuron is permitted to make self-connections, the diagonal entries of S are given by $S_{i=j} \equiv s_{ii} = \{\mathrm{E}[g_D]\cdot(N-1) + 1\}^{-1}$. Equations (A8) can be evaluated numerically by taking the natural logarithm of both sides. Due to the correlations introduced by the symmetric structure of S, tighter estimates for $\mathrm{E}\lceil\Sigma_L S_{i\neq j}\rceil$ and $\mathrm{E}\lfloor\Sigma_L S_{i\neq j}\rfloor$ can be obtained by replacing $\sigma_{g_D}^2$ with $\sigma_{g_D}^2/(1 + 2D^{-1})$ when deriving parameters for Eqs. (A8).

APPENDIX B: ANALYSIS OF INDIVIDUAL COMPONENTS OF EQ. (10)

The estimated upper real bound of the eigenspectrum for a matrix W describing a network with spatial and functional constraints (i.e., $\kappa < \infty$) is given in Eq. (10) as

$$2\lceil\lambda_+\rceil = \lceil\hat{w}_{ee}\rceil - \lfloor\hat{w}_{ii}\rfloor + [(\lceil\hat{w}_{ee}\rceil + \lfloor\hat{w}_{ii}\rfloor)^2 - 4\lceil\hat{w}_{ei}\rceil\lfloor\hat{w}_{ie}\rfloor]^{\frac{1}{2}}. \tag{B1}$$

The distributions for $\hat{w}_*$ in Eq. (B1) are analytic, and can be more readily related to the parameters defining the network connectivity if one recognizes that each of $\hat{w}_*$ is a function of D and κ, related through sums of the spatial constraint matrix S. For example, $\hat{w}_{ee}(\kappa, D) \approx w_E[s_{ii}(\kappa, D) + \Sigma_{(1-f_I)N-1}S(\kappa, D)]$, and similarly for the other $\hat{w}_*$. The explicit values for each extremal estimate used to calculate $\lceil\lambda_+\rceil$ in Eqs. (10) and (B1)

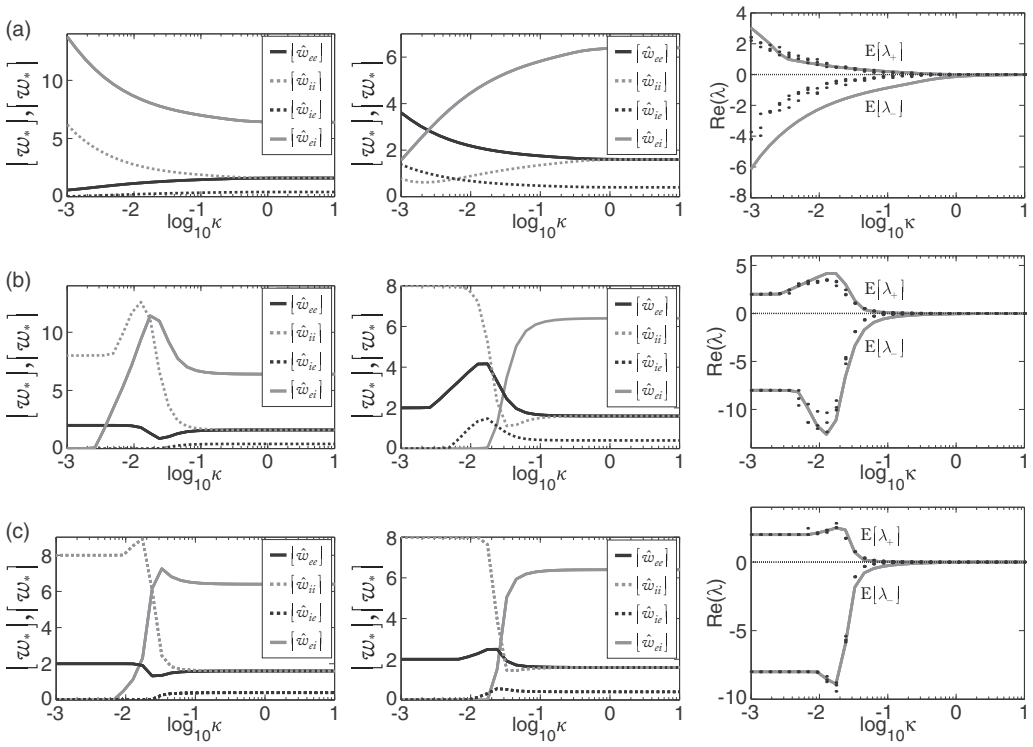

FIG. 4. Plots of extremal weight component estimates $\hat{w}_*$ used to calculate $\mathrm{E}\lceil\lambda_-\rceil$ (left column) and $\mathrm{E}\lfloor\lambda_+\rfloor$ (middle column). At right are shown analytical estimates for $\mathrm{E}\lceil\lambda_+\rceil$ and $\mathrm{E}\lfloor\lambda_-\rfloor$ (gray curves), as well as the empirical λ_+ and λ_- (black dots) computed numerically for many instances of W. For all panels $r = 0$, h_I, $h_E = 1$, $N = 6000$, $w_E = 2$, $w_I = 8$, and $f_I = 20\%$. Values for D: (a) 1, (b) 5, (c) 10. A comparison between predicted and empirical λ_+ and λ_- for $D = 2$ is shown in Fig. 2(b).

are given by

$$\begin{aligned}
\lceil\hat{w}_{ee}(\kappa,D)\rceil &= w_E\{s_{ii}(\kappa,D) + \mathrm{E}\lceil\Sigma_{(1-\mathrm{f_I})\mathrm{N}-1}\mathrm{S}(\kappa,\mathrm{D})\rceil\},\\
\lfloor\hat{w}_{ii}(\kappa,D)\rfloor &= w_I\{s_{ii}(\kappa,D) + \mathrm{E}\lfloor\Sigma_{f_I N-1}S(\kappa,D)\rfloor\},\\
\lfloor\hat{w}_{ie}(\kappa,D)\rfloor &= w_I\cdot\mathrm{E}\lfloor\Sigma_{(1-f_I)N}S(\kappa,D)\rfloor,\\
\lceil\hat{w}_{ei}(\kappa,D)\rceil &= w_E\cdot\mathrm{E}\lceil\Sigma_{f_I N}S(\kappa,D)\rceil,
\end{aligned} \tag{B2}$$

where $\mathrm{E}[\cdot]$ is the expectation operator and with the maximum and minimum extremal distributions denoted by $\lceil\cdot\rceil$ and $\lfloor\cdot\rfloor$, as in the main text. Expressions for $s_{ii}(\kappa,D)$ and for $\Sigma_L S(\kappa,D)$ are given in Appendix A and in the main text. Figure 4 illustrates how the values of $\hat{w}_*$, $\mathrm{E}\lceil\lambda_+\rceil$, and $\mathrm{E}\lfloor\lambda_-\rfloor$ vary depending on the dimensionality of the network D and on the spatial range parameter κ.

Matlab code is available to generate the family of matrices defined in this paper [48].

[1] R. H. R. Hahnloser, Neural Networks **11**, 691 (1998).
[2] K. Rajan and L. F. Abbott, Phys. Rev. Lett. **97**, 188104 (2006).
[3] D. B. Larremore, W. L. Shew, and J. G. Restrepo, Phys. Rev. Lett. **106**, 058101 (2011).
[4] A. Landsman, E. Neftci, and D. R. Muir, New J. Phys. **14**, 123031 (2012).
[5] G. Wainrib and J. Touboul, Phys. Rev. Lett. **110**, 118101 (2013).
[6] S. Ostojic, Nature Neuroscience **17**, 594 (2014).
[7] U. Rutishauser and R. J. Douglas, Neural Computation **21**, 478 (2009).
[8] H. R. Wilson and J. D. Cowan, Kybernetik **13**, 55 (1973).
[9] H. J. Tang and K. C. Tan, Neural Computation **17**, 97 (2005).
[10] D. R. Muir and M. Cook, Neural Computation **26**, 1624 (2014).
[11] V. L. Girko, Theory of Probability and its Applications **29**, 694 (1984).
[12] H. J. Sommers, A. Crisanti, H. Sompolinsky, and Y. Stein, Phys. Rev. Lett. **60**, 1895 (1988).
[13] Y. Wei, Phys. Rev. E **85**, 066116 (2012).
[14] S. K. Dwivedi and S. Jalan, Phys. Rev. E **87**, 042714 (2013).
[15] C. D. Gilbert and T. N. Wiesel, J. Neurosci. **9**, 2432 (1989).
[16] A. Burkhalter and K. L. Bernardo, Proc. Natl. Acad. Sci. USA **86**, 1071 (1989).
[17] S. L. Juliano, D. P. Friedman, and D. E. Eslin, Journal of Comparative Neurology **298**, 23 (1990).
[18] R. Malach, Y. Amir, M. Harel, and A. Grinvald, Proc. Natl. Acad. Sci. USA **90**, 10469 (1993).
[19] W. H. Bosking, Y. Zhang, B. Schofield, and D. Fitzpatrick, J. Neurosci. **17**, 2112 (1997).
[20] Y. Yoshimura, J. L. M. Dantzker, and E. M. Callaway, Nature (London) **433**, 868 (2005).

[21] H. Ko, S. B. Hofer, B. Pichler, K. A. Buchanan, P. J. Sjöström, and T. D. Mrsic-Flogel, Nature (London) **473**, 87 (2011).
[22] D. R. Muir, N. M. A. Da Costa, C. Girardin, S. Naaman, D. B. Omer, E. Ruesch, A. Grinvald, K. A. Martin, and R. J. Douglas, Cerebral Cortex **21**, 2244 (2011).
[23] N. Geard and J. Wiles, Artificial Life **11**, 249 (2005).
[24] H. Nakao and A. S. Mikhailov, Nat. Phys. **6**, 544 (2010).
[25] T. Binzegger, R. J. Douglas, and K. A. C. Martin, J. Neurosci. **24**, 8441 (2004).
[26] M. Girvan and M. E. J. Newman, Proc. Natl. Acad. Sci. USA **99**, 7821 (2002).
[27] Y. Li, H. Lu, P.-l. Cheng, S. Ge, H. Xu, S.-H. Shi, and Y. Dan, Nature (London) **486**, 118 (2012).
[28] M. Mézard, G. Parisi, and A. Zee, Nuclear Physics B **559**, 689 (1999).
[29] A. Amir, Y. Oreg, and Y. Imry, Phys. Rev. Lett. **105**, 070601 (2010).
[30] S. E. Skipetrov and A. Goetschy, J. Phys. A **44**, 065102 (2011).
[31] C. Holmgren, T. Harkany, B. Svennenfors, and Y. Zilberter, Journal of Physiology **551**, 139 (2003).
[32] T. Binzegger, R. J. Douglas, and K. A. C. Martin, J. Neurosci. **27**, 12242 (2007).
[33] C. Boucsein, M. P. Nawrot, P. Schnepel, and A. Aertsen, Frontiers in Neuroscience **5**, 32 (2011).
[34] D. H. Hubel and T. N. Wiesel, Journal of Physiology (London) **160**, 106 (1962).
[35] S. Chauhan, M. Girvan, and E. Ott, Phys. Rev. E **80**, 056114 (2009).
[36] G. Ergün and R. Kühn, J. Phys. A **42**, 395001 (2009).
[37] R. Kühn and J. van Mourik, J. Phys. A **44**, 165205 (2011).
[38] T. P. Peixoto, Phys. Rev. Lett. **111**, 098701 (2013).
[39] F. McSherry, in *Proceedings of the 42nd IEEE Symposium on Foundations of Computer Science, 2001* (IEEE, Piscataway, 2001), pp. 529–537.
[40] C. Gkantsidis, M. Mihail, and E. Zegura, in *Twenty-Second Annual Joint Conference of the IEEE Computer and Communications, IEEE Societies, INFOCOM 2003* (IEEE, Piscataway, 2003), Vol. 1, pp. 364–374.
[41] R. R. Nadakuditi and M. E. J. Newman, Phys. Rev. Lett. **108**, 188701 (2012).
[42] Y. Ahmadian, D. B. Rubin, and K. D. Miller, Neural Computation **25**, 1994 (2013).
[43] D. B. Rubin, S. D. Van Hooser, and K. D. Miller, Neuron **85**, 402 (2015).
[44] R. Coultrip, R. Granger, and G. Lynch, Neural Networks **5**, 47 (1992).
[45] A. Goetschy and S. E.. E. Skipetrov, Phys. Rev. E **84**, 011150 (2011).
[46] S. O. Rice, Bell System Technical Journal **23**, 282 (1944).
[47] C. G. Koay and P. J. Basser, J. Magn. Reson. **179**, 317 (2006).
[48] See Supplemental Material at http://link.aps.org/supplemental/10.1103/PhysRevE.91.042808 for code used to generate and analyze the families of matrices defined in this paper.